Available online at www.sciencedirect.com

ScienceDirect

Acta Materialia 69 (2014) 343–354

Acta MATERIALIA

www.elsevier.com/locate/actamat

Full icosahedra dominate local order in $Cu_{64}Zr_{34}$ metallic glass and supercooled liquid

Jun Ding [a], Yong-Qiang Cheng [b], Evan Ma [a,*]

[a] Department of Materials Science and Engineering, Johns Hopkins University, Baltimore, MD 21218, USA
[b] Chemical and Engineering Materials Division, Oak Ridge National Laboratory, Oak Ridge, TN 37831, USA

Received 11 November 2013; received in revised form 30 January 2014; accepted 3 February 2014
Available online 9 March 2014

Abstract

Extensive molecular dynamics simulations were carried out to monitor the development of icosahedral order in $Cu_{64}Zr_{34}$ liquid and metallic glass (MG). This study illustrates that at this Cu-rich Cu–Zr alloy composition, Cu-centered full icosahedra constitute the dominant and characteristic short-range-ordered coordination motif. The results for this model liquid/glass address five questions regarding the ordering of Cu-centered coordination polyhedral towards full icosahedra, including: (i) its evolution and extent during prolonged structural relaxation; (ii) the resulting reduction in potential energy and slowing-down of dynamics; (iii) the accompanying preference of a particular type of Zr-centered Kasper coordination polyhedra; (iv) the evolution and conversion of polyhedral connection schemes in the medium range; and (v) the formation and percolation of networks formed by interpenetrating connection of icosahedra to constitute a stiff backbone over extended range. Five related issues are also clarified, to: (i) differentiate full-icosahedra-based ordering from the generally favorable fivefold bonds; (ii) compare the Cu-based perspective with a Zr-centric view; (iii) systematically list the rationales behind focusing on icosahedral order for explaining the $Cu_{64}Zr_{34}$ MG/liquid properties; (iv) discuss other non-icosahedral ordering varieties; and (v) comment on the most liquid-like local environments. Taken together, the ten issues addressed set the stage for understanding structure–property relations in a category of amorphous alloys that can be characterized based on full-icosahedral ordering.

Keywords: Metallic glasses; Supercooled liquids; Full icosahedra; Cu–Zr

1. Introduction

Metallic glasses (MGs) and their parent liquids are characterized by an amorphous structure with no long-range order [1–5]. The internal structure of these materials, therefore, needs to be understood at an atomic level [6–9]. In particular, a meaningful description of the local order, in terms of characteristic short-to-medium-range features [6–8], is desirable. Obviously, this is a highly challenging proposition. In general, metallic bonds have minimal directionality, such that, to lower energy, there should be a tendency to surround any given (center) atom with as many bonding neighbors as possible. Regarding this efficient use of space, tetrahedral packing is advantageous, because each atom in the tetrahedron is in contact with all the other three atoms. The polytetrahedral packing model [10] is therefore widely embraced. One sub-category of such packing, in the case of packing 12 atoms around a center atom (when the coordination number is 12, CN = 12), is icosahedral packing [10]. This is an efficient way of maximizing tetrahedral atomic arrangements and triangulated shell faces: the 12 shell atoms form an icosahedron composed of 20 tetrahedra. The geometrically perfect/ideal icosahedron has a slightly smaller A atom at the center, surrounded by shell atoms of the same kind (B), at an atomic size ratio (A to

* Corresponding author.
E-mail address: ema@jhu.edu (E. Ma).

http://dx.doi.org/10.1016/j.actamat.2014.02.005
1359-6454/

B) of 0.902 [11]. Such an icosahedron is actually more centrosymmetric, and establishes more bonds than the 13-atom face centered cubic/hexagonal close packed (fcc/hcp) cluster. Icosahedra could be the featured local structure in amorphous metals, as originally postulated by Frank for monoatomic liquids [12].

Indeed, in recent years, many experimental studies (e.g. [6,13–18]) using X-ray/neutron scattering and nanobeam electron diffraction, as well as numerous computer simulations employing ab initio or empirical interatomic interactions (e.g. [6,19–22]), have identified local icosahedral order in metallic liquids and glasses. Of course, the icosahedra detected are not the prototypical ideal icosahedra mentioned earlier that have 20 identical and almost equilateral tetrahedra (edges formed between neighboring shell atoms are slightly longer). Instead, the icosahedra are distorted to various degrees; this is because, in a real MG/liquid, the center-to-shell atomic size ratio is not exactly 0.902, the average CN deviates slightly from 12, and the glass/liquid is often a concentrated alloy such that the shell is composed of both A and B atoms of different sizes. In recent publications [8,19–21], the present authors defined a category of CN = 12 Cu-centered clusters as "full icosahedra". These Cu-centered full icosahedra (Cu-FI) have a Voronoi index of $\langle 0,0,12,0\rangle$. That is, the icosahedral motif is "complete" in the sense that the center Cu has all the 12 neighbors that enclose an icosahedron, and all the 12 bonds are fivefold bonds, even though the cluster is not unique, but consists of a range of quasi-equivalent configurations featuring the same CN and Voronoi index. This Cu-FI designation differentiates them from fragments of icosahedra, heavily distorted icosahedra-like polyhedra (e.g. those with Voronoi index $\langle 0,2,8,2\rangle$, $\langle 0,3,6,3\rangle$ or even $\langle 0,2,8,1\rangle$) or merely bond-pairs with a fivefold environment (see additional discussions in Section 4.1). While all these varieties have been reported in the literature as evidence of icosahedral short-range order (ISRO), the full-icosahedra short-range ordering (FISRO) that the present authors singled out is arguably the tell-tale signature of ISRO and often the most property-controlling structural indicator [8,19–23].

There are, however, a number of unresolved issues regarding FISRO in MGs and liquids. This study touches on 10 such questions. The presentation in this paper is arranged as follows. After the methods section (Section 2), Section 3 presents the results of a systematic molecular dynamics (MD) simulation study looking into the FISRO development in a Cu-rich amorphous alloy, $Cu_{64}Zr_{34}$; at this alloy composition Cu-FI are known to be highly populous for Cu-centered coordination polyhedral [24]. Using this model liquid/glass, the study addresses five questions regarding FISRO that have so far not been adequately explored, beginning with a query on the extent of FISRO. The constructed glass structure based on experimental data from laboratory MGs relied on the Reverse Monte Carlo (RMC) method [6]. But the RMC samples the configurational space in a random manner, such that the final configuration reached is essentially the most random structure that can reproduce/fit the target experimental input within a given tolerance. As a result [17], the fraction of Cu in centers of FI is even less than that given by computer simulations conducted at very fast quench rates. The first pending question therefore concerns the potential extent/degree of FISRO. To monitor the (possibly significant) further development of FISRO, the MD simulations are purposely prolonged by cooling the liquid at a relatively slow quench rate (10^9 K s^{-1}) and aging the supercooled liquid at 800 K for as long as >300 ns. Second, the evolution of configurational potential energy (CPE) of the alloy is monitored, along with the extensive structural evolution inside, to shed light on the driving force for pronounced FISRO at this alloy composition. Third, previous studies examined the Cu–Zr MG structure from the perspective of the dominant Cu-centered clusters. It was believed that the behavior of the Zr environment is relatively featureless [8], with a broad distribution of many cluster types, each accounting for only a few per cent of all the Zr atoms. With the prolonged simulation, it is now possible to identify the preferential development of certain Zr-centered Frank–Kasper coordination polyhedra [25]. The fourth question addresses the development of extended icosahedra ordering. As enormous Cu-FI clusters permeate the system with aging and/or slow cooling, one gets a better feel as to how the Cu-FI connect to one another, and how connection schemes in the medium range (second neighbors) evolve and convert to one another, as a function of decreasing temperature during supercooling, and over a range of cooling rates. Fifth, the large numbers of Cu-FI provide the opportunity for us to monitor the formation and percolation of networks formed by interpenetrating connection of icosahedra (ICOI) [26]. This extended icosahedral ordering is shown to play a role in constituting a stiff backbone and elevating the shear modulus of the glass.

Section 4 addresses five additional issues. These questions naturally emerge from the storyline presented in Section 3. First, the definition of ISRO is further clarified: in particular, the FISRO based on Cu-FI vs. the presence/population of fivefold bonds. It is emphasized that FISRO dominates only in a limited number of alloys (at certain MG compositions), while fivefold bonds and triangulated shell faces are always preferred across the board for all MGs/liquids. Second, after much discussion on Cu-centered motifs, one is naturally curious about a comparison with a characterization of the MG structure from a Zr-centric perspective (or by taking a global average of all atoms). Third, the rationales behind focusing on Cu-FI as the characteristic SRO for the $Cu_{64}Zr_{34}$ MG/liquid are discussed, as well as the reasons for explaining MG/liquid properties from the FISRO standpoint. Fourth, the present authors briefly comment on the non-FISRO ordering types, e.g. the other preferable types of polytetrahedral clusters/motifs at other Cu–Zr compositions and in other amorphous alloy systems. The fifth and final question, which is discussed briefly, is the coordination environments at the opposite extreme: those that are the furthest away from

FI. These are the least ordered local structures, or fragmented motifs, and low in population. But such unfavorable and uncomfortable local environments also deserve attention, as they can be relevant or even controlling for certain important properties.

2. Methods

The present work employs MD simulations to study $Cu_{64}Zr_{36}$ model systems. They are simulated by optimized embedded atom method (EAM) potential, adopted from Ref. [19]. Each sample contains 32,000 atoms, and the liquids of those samples were equilibrated for 10 ns at high temperature (2500 K) to ensure equilibrium, and were then quenched to room temperature (300 K) at cooling rates of 10^9–10^{12} K s^{-1} under a Nose–Hoover thermostat (the external pressure was barostatted at zero) [27]. The periodic boundary condition is applied in all three directions. Another simulation procedure was to cool the liquid to 800 K at the cooling rate of 10^{12} K s^{-1}, and then hold the supercooled liquid for structural relaxation (under a *NPT* ensemble) at that temperature for 300 ns before quenching to room temperature. The time step used in all the simulations was 2 fs. Smaller $Cu_{64}Zr_{36}$ samples with 10,000 atoms via Mendelev's Finnis–Sinclair EAM potential [28] were also quenched at 10^9 K s^{-1} and 10^{10} K s^{-1}, following the procedure presented above.

The local coordination in $Cu_{64}Zr_{36}$ liquids and MGs is monitored by conducting Voronoi analysis on their corresponding inherent structures. The Voronoi tessellation [29] is a scheme to divide the three-dimensional space into cells centered by each atom. A plane is drawn to bisect each line connecting the center atom and one of the neighboring atoms, and the cell enclosed by all the inner planes is called a Voronoi cell, which encloses the part of space that is closer to the center atom than any other atoms. This method can be used to unambiguously determine the CN without the need for a cutoff: those and only those atoms sharing a common cell surface are considered nearest neighbors. For MGs with more than one species, the bisection can be weighted by the atomic size. Faces of Voronoi cell with area <0.25% of the total area are discounted. The four-number Voronoi index, $\langle i_3, i_4, i_5, i_6\rangle$, describes the arrangement and topology of the nearest-neighbor atoms around the center atom. Specifically, i_3 represents the number of triangles on the Voronoi polyhedron, i_4 the number of quadrangles, i_5 the number of pentagons, and i_6 the number of hexagons. The connection schemes of coordination polyhedra are also assessed, and are described in later sections.

The isothermal stiffness coefficients (C) at room temperature were evaluated using the fluctuation method [30–32]. For a canonical (*NVT*) ensemble, C can be calculated as the sum of three contributions [31]

$$C^T_{ijkl} = C^{\mathrm{I}}_{ijkl} + C^{\mathrm{II}}_{ijkl} + C^{\mathrm{III}}_{ijkl} \quad (1)$$

where the superscripts I, II and III represents the fluctuation, kinetic contribution and the Born term, respectively (see Ref. [31] for more details). To reduce the statistical error in the simulated samples, the average shear modulus (G) was evaluated as

$$G = \frac{C_{44} + C_{55} + C_{66}}{3} \quad (2)$$

G can also be decomposed into three terms corresponding to those in Eq. (1). For instance,

$$G^{\mathrm{I}} = \frac{C^{\mathrm{I}}_{44} + C^{\mathrm{I}}_{55} + C^{\mathrm{I}}_{66}}{3} \quad (3)$$

To evaluate local elasticity, the simulation box is subdivided into a grid of $90 \times 90 \times 90$ following Ref. [32–34] and the local elastic moduli tensor C^{ξ}_{ijkl} at the center of each subcell ξ is computed on a coarse-grained scale using Gaussian with full width at half maximum of 8 Å. The average local elastic modulus tensor would be equal to the global elastic tensor [32]. Using this approach, the local shear modulus C^{ξ}_{44} can be plotted with adequate spatial resolution to reflect its heterogeneous distribution.

3. Results and discussion

3.1. The extent of FISRO

Fig. 1a plots the fractions of Cu atoms that center different coordination polyhedra, out of all the Cu atoms in the alloy, as a function of temperature during cooling of the $Cu_{64}Zr_{36}$ liquid at the slowest cooling rate (10^9 K s^{-1}) used in this study. It is observed that the dominant CN is 12, and the FISRO development takes off in the supercooled liquid region. The trend is obviously that Cu-FI is the group that exhibits the most pronounced rise, relative to the other competing Cu-centered coordination polyhedra in Fig. 1a. The fraction of Cu atoms centering FI reached as high as 40% of all Cu atoms in the alloy; and since each FI involves 13 atoms (12 Cu and Zr atoms in the shell), these Cu-FI quasi-equivalent clusters involve as much as 90% of all the (Cu + Zr) atoms in the system. To make sure that the finding is not borne out of a particular interatomic potential, the fraction of Cu-FI in a $Cu_{64}Zr_{36}$ liquid/MG obtained using the Mendelev potential was also monitored [28]. A data point is included in Fig. 1a for comparison. While the latter potential produces a slightly lower fraction of icosahedra, a very similar trend is observed. The structure factors of simulated $Cu_{64}Zr_{36}$ glasses are displayed in Fig. 1c, to show that they are consistent with X-ray diffraction data for $Cu_{64.5}Zr_{35.5}$ glass in experiment [28].

Similar structural evolution towards extensive FISRO is also observed on aging the $Cu_{64}Zr_{36}$ supercooled liquid at 800 K. The relaxation time at this temperature was extended to 300 ns, which is exceedingly long when compared with all previous MD simulations (the typical quench rate used before was >10^{10} K s^{-1}, with a total simulation time of no more than a few nanoseconds over the temperature range in the supercooled liquid region), before cooling down to room temperature. As shown in Fig. 2a,

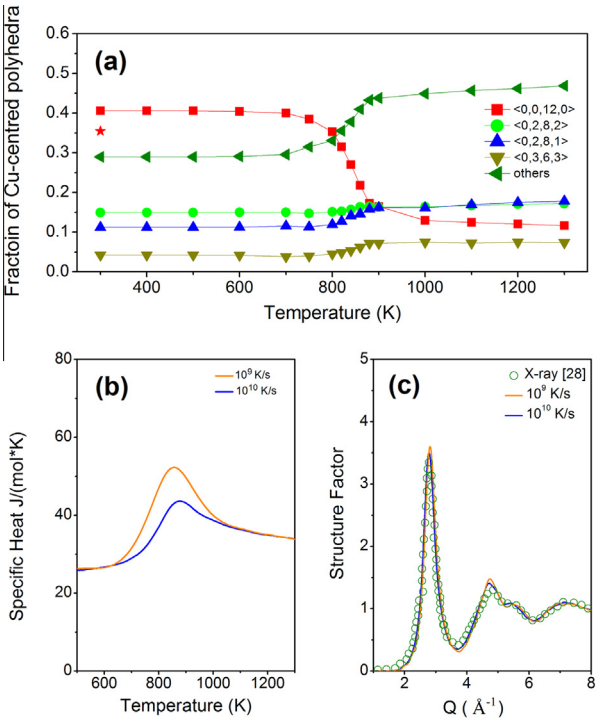

Fig. 1. (a) Temperature dependence of the fractions of Cu-centered coordination polyhedra. Solid star is for the fraction of Cu-centered icosahedra in $Cu_{64}Zr_{36}$ glasses obtained with the cooling rate of 10^9 K s^{-1} using Mendelev's potential [28]. (b) Temperature dependence of specific heat for $Cu_{64}Zr_{36}$ with cooling rates of 10^9 and 10^{10} K s^{-1} from supercooled liquids to glassy states. (c) Structure factor of simulated $Cu_{64}Zr_{36}$ glasses with comparison with X-ray diffraction of $Cu_{64.5}Zr_{35.5}$ glass in experiment [28].

among all the Cu-centered coordination polyhedra, the only type that experienced persistent and pronounced increase in population is the Cu-FI. Similar to the continuous cooling case, the fraction of Cu atoms centering FI is now 41% of all Cu atoms in the alloy, far exceeding that previously reported for this alloy [8]. FISRO based on Cu-FI is clearly the dominant local motifs in $Cu_{64}Zr_{36}$ supercooled liquid and MG.

3.2. The role of FISRO in reducing energy and slowing down dynamics

Having confirmed the progressive development of FISRO in "slowly cooled" or "aged" $Cu_{64}Zr_{36}$, the second point to ascertain is that FISRO indeed brings down the system energy. This point is made in Figs. 1b and 2b. Indeed, the steep rise in Cu-FI during undercooling in Fig. 1a apparently coincides with the fast increase in specific heat (the derivative of system energy with respect to temperature) with cooling in Fig. 1b, which was also revealed in earlier studies [20,35]. Since Cu is the majority species, the system energy reduction during structural evolution is expected to go hand in hand with the decreasing CPE of the Cu atoms. In Fig. 2b for the aging experiment at 800 K, the pronounced increase in Cu-FI observed in Fig. 2a also correlates very well with a continuously decreasing CPE of the alloy. These results suggest that it is the pronounced reduction in CPE due to the topological and chemical ordering associated with the formation of Cu-FI that drives the preferential conversion of other viable local environments towards FISRO (see Fig. 1).

To further establish the critical role of FISRO, the pronounced development of Cu-FI in supercooled $Cu_{64}Zr_{36}$ liquid also has the consequence of slowing down the dynamics of the cooling liquid. Indeed, as shown in Fig. 3, the average bond lifetime τ_{delay}, which measures the delay time for the breakage of an atomic bond (as defined in Ref. [36]) for $Cu_{64}Zr_{36}$ supercooled liquids under structural relaxation at 800 K, is observed to increase by orders of magnitude, owing to the increased fraction of Cu-FI. Fig. 4 plots the spatial distribution of bond lifetime for all atoms in a slice of $Cu_{64}Zr_{36}$ supercooled liquid (with 35% Cu-FI) at 800 K. The slice has a layer thickness of ~2.5 Å (roughly equal to atomic spacing). The colors in the plot denote the bond lifetime in logarithmic scale, see corresponding sidebar for τ_{delay}, in $\log_{10}\tau_{delay}$ (picosecond). The open circles are for Cu atoms at the centers of full icosahedra. There is clearly a strong correlation between the two: regions with slow dynamics are statistically more enriched in Cu-FI (correspondingly, the bond lifetime inversely scales with the fraction/population of non-icosahedral Cu-centered polyhedra). This is another indicator of the important role of FISRO in contributing to the overall properties of the alloy, i.e. clear evidence of structural relaxation (viscosity) correlating with local atomic arrangements.

3.3. Zr-centered Z16 Kasper polyhedra

The extensive aging afforded the opportunity to resolve a third question, namely, the preferential development of a specific type of coordination polyhedra around Zr. Fig. 2c shows that the preferred CN moves towards 16 around Zr. The motif favorable for CN = 16 has been predicted to be the $\langle 0,0,12,4\rangle$ polyhedra (Z16 cluster), which is the configuration with the lowest disclination content [8]. But instead, $\langle 0,1,10,4\rangle$ and $\langle 0,1,10,5\rangle$ were observed in earlier studies to be relatively more populous in $Cu_{64}Zr_{36}$, and the Zr atoms centering these coordination polyhedra only amount to 10–13% of all the Zr atoms [8]. As shown in Fig. 2c, this dilemma is now resolved: given sufficiently long relaxation, the $\langle 0,0,12,4\rangle$ Kasper polyhedra indeed take over to become the most populous, reaching a fraction of 17% of all Zr-centered polyhedra. As expected, the evolution towards favorable Kasper polyhedra holds for the two species in the alloy: the rise of Z16 polyhedra goes hand in hand with the escalating population of Cu-FI, as shown in the almost linear correlation (on sufficient relaxation) between the two (Fig. 2d). Together, they reduce the density of extrinsic disclinations [8] for more regular polytetrahedral packing.

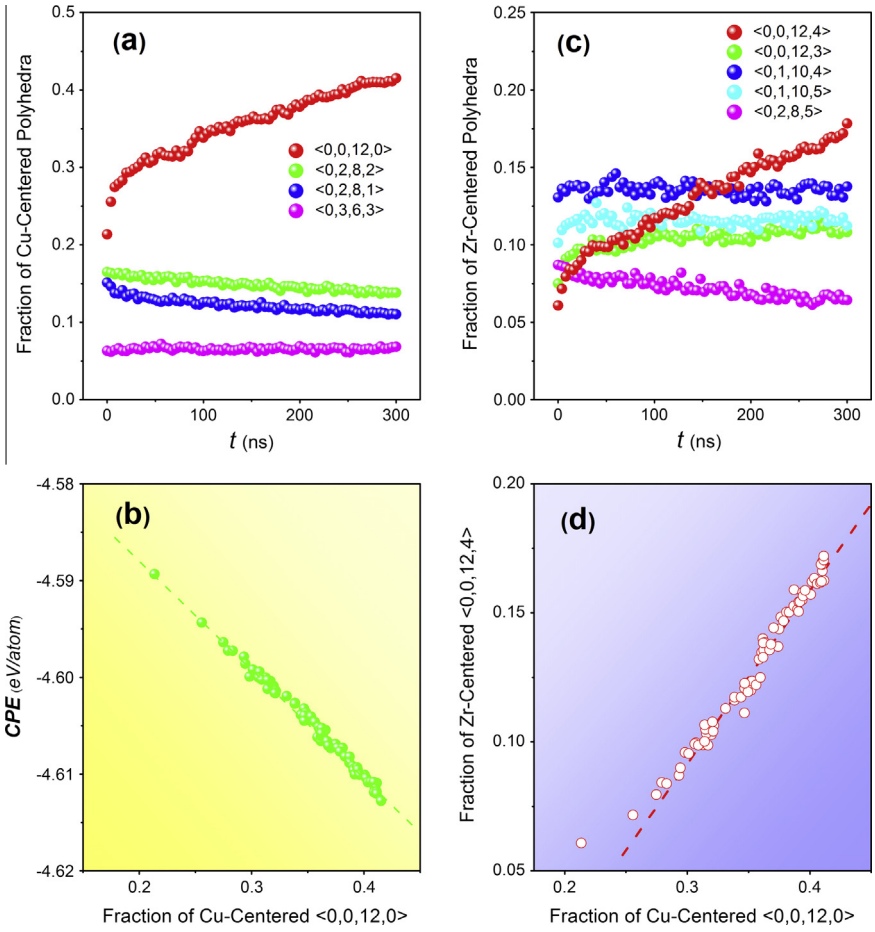

Fig. 2. Structural relaxation of $Cu_{64}Zr_{36}$ supercooled liquids at 800 K: (a) fractions of Cu-centered coordination polyhedra; (b) correlation between the fraction of Cu-FI and configurational potential energy of the alloy; (c) fractions of Zr-centered coordination polyhedra; (d) correlation between the fractions of Cu-centered $\langle 0,0,12,0\rangle$ and Zr centered $\langle 0,0,12,4\rangle$.

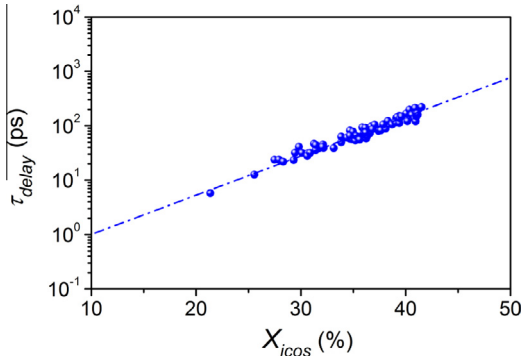

Fig. 3. Relationship between the fraction of Cu-centered icosahedra (X_{icos}) and average bond lifetime (τ_{delay}) in $Cu_{64}Zr_{36}$ supercooled liquid under structural relaxation at 800 K.

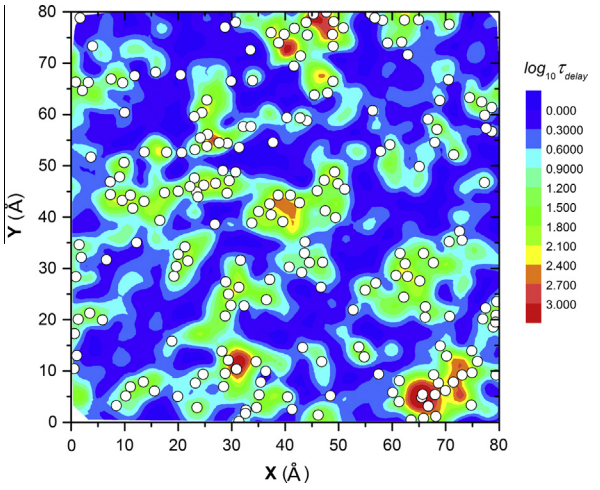

Fig. 4. Spatial distribution of bond lifetime for all atoms in a slice of $Cu_{64}Zr_{36}$ supercooled liquid (with 35% Cu-centered icosahedra) at 800 K. The slice has a layer thickness of ~2.5 Å (roughly equal to atomic spacing). The colors denote the bond lifetime in logarithmic scale; see corresponding sidebar for $\log_{10}(\tau_{delay})$ in picosecond. The open circles are for Cu atoms at the centers of full icosahedra. (For interpretation of the references to color in this figure legend, the reader is referred to the web version of this article.)

3.4. Evolution of polyhedra connections in the medium range

The extended ordering is now monitored in terms of the connection schemes that link the short-range-ordered polyhedra together. Here, two basic types, which are simultaneously present in the alloy, are analyzed. The first type is a Cu-centered full icosahedron overlapping with another

Cu-centered full icosahedron; this scenario is termed "interpenetrating connection of icosahedra" (ICOI) [26,37,38]. Here, the latter Cu atom, while being the center of another full icosahedron, is a nearest neighbor of the former Cu. Such a connection joins FI together, to build networks of FI that eventually constitutes the backbone of the glass (see Section 3.5). The second type is more general, concerning the connection schemes that link any two Cu-centered coordination polyhedra [19,35], where the two center atoms are second nearest neighbor (see below). A consideration of these two connection types thus reveal certain aspects of correlations over the medium range, i.e. beyond nearest-neighbor atoms and extending to first-neighbor and second-neighbor polyhedral motifs.

For the first type, Fig. 5 presents the fraction of interpenetrating icosahedra out of all the surrounding Cu, on average for each Cu full icosahedron. As expected, the former increases fast with increasing fraction of Cu-FI. Apparently, the measured fraction of interpenetrating icosahedra is much higher than that expected from a random distribution of Cu-FI (see the orange solid line). This indicates that the Cu-FI tend to aggregate, at least in the short-to-medium range, as building blocks of the amorphous structure [6]. This role of ICOI is discussed further in Section 3.5. Meanwhile, the separated Cu-FI without interpenetrating connection (right y axis in Fig. 5) become fewer with increasing fraction of Cu-FI.

For the second type, the connection schemes examined here cover a wide range, including vertex sharing (VS), edge sharing (ES) and face sharing (FS). In these three cases, the two neighboring atomic clusters share 1, 2 and 3 atoms, respectively, as shown schematically in the insets in Fig. 6a. For the two Cu atoms at the centers, they are second nearest neighbor in all these schemes (see schematics in Fig. 6a). In Fig. 6a, the evolution of Cu–polyhedra connections is plotted as a function of temperature, during cooling from the liquid state to the glassy state. Three different cooling rates, 10^9 K s^{-1}, 10^{10} K s^{-1} and 10^{12} K s^{-1}, are compared. The corresponding curves, from the slowest to the fastest cooling rate in the direction of the arrow, are displayed together. The degree of ES and FS evolves with increasing supercooling in the liquid [35]: FS increases, while ES decreases. Also, a slower cooling rate, in other words more structural relaxation, leads to more pronounced growth of FS and reduction of ES. The steep rise of FS in the supercooled liquid region as T approaches T_g is analogous to the behavior of FISRO reported in Fig. 1a. The total number of connections to other motifs (between centered Cu as second nearest neighbor) does not change significantly, because the increase in FS connections appears to be accompanied by the reduction in ES connections. In sum, structural relaxation during supercooling

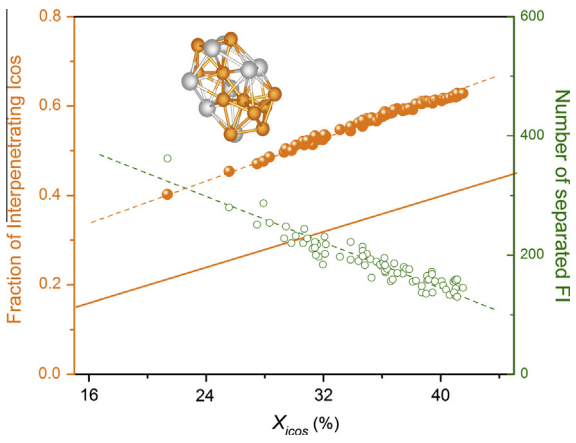

Fig. 5. The rising fraction of ICOI per Cu-centered full icosahedron (left y axis, orange symbols) scales with the fraction of Cu-centered icosahedra. The solid orange line represents the situation of random distribution of icosahedra. Inset is a schematic showing a segment of ICOI (gray atoms are Zr, and yellow ones are Cu). Correspondingly, the number of separated Cu-centered icosahedra (right y axis, without interpenetrating connection with surrounding icosahedra) decreases with increasing X_{icos}. (For interpretation of the references to color in this figure legend, the reader is referred to the web version of this article.)

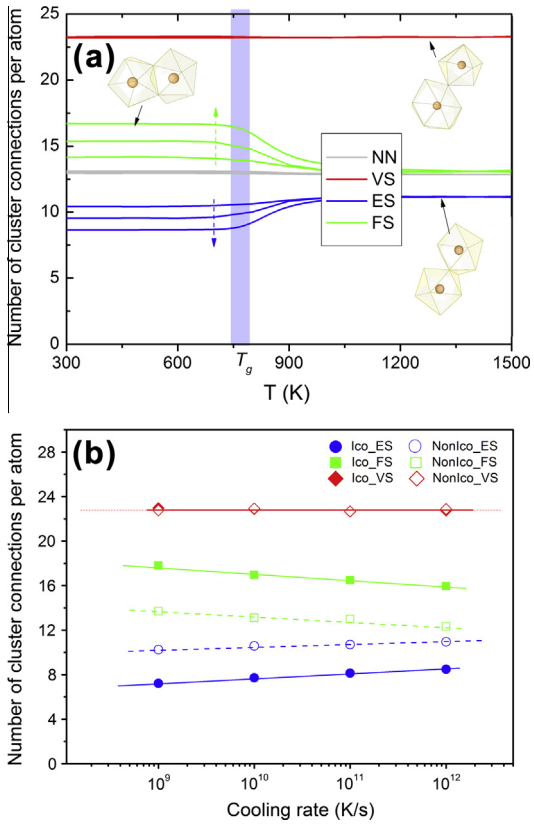

Fig. 6. (a) The evolution (temperature dependence) of average number of nearest neighbors (NN) for Cu-centered coordination polyhedra connected via various schemes in $Cu_{64}Zr_{36}$ supercooled from the liquid state to the glass state. Samples were cooled at 10^9, 10^{10} and 10^{12} K s^{-1}, respectively, and the increasing cooling rate is marked by a dashed arrow. The blue-shaded bar marks the glass transition temperature. Schematic description of VS, ES and FS are included. (b) The average number of connected clusters for Cu-centered icosahedra and non-icosahderal coordination polyhedra in $Cu_{64}Zr_{36}$ MGs obtained at various cooling rates. (For interpretation of the references to color in this figure legend, the reader is referred to the web version of this article.)

leads to the growth of the more favorable FS connection, at the expense of ES. In contrast, the average number of VS connections per atom experiences little change from 1500 K to 300 K, perhaps because VS exerts little additional atomic stress, owing to the longer distance between the centers of the two connecting clusters.

The same trend, i.e. the increasing FS vs. decreasing ES during supercooling, is observed for both Cu-FI and non-icosahedral Cu-centered polyhedra (Cu-non-FI). But the difference is that the average number of FS connections to a Cu-FI is greater than that around a Cu-non-FI, by as much as ~4. This is shown in Fig. 6b, in the eventual glass formed by cooling from the liquid state at different rates. It demonstrates that, compared with all other Cu-centered polyhedra types, Cu-FI are better connected (with clusters each centered by a second-neighbor Cu in this case) by transforming more ES to FS, again lending support to the role of FISRO in forming more stable/slow regions (see Section 3.5).

3.5. Percolation of ICOI networks: effect on shear modulus

The study now proceeds to examine the connection of Cu-FI over further extended ranges. Section 3.2 discussed the role of FISRO in slowing down the dynamics of supercooled liquids. This section moves onto the MGs, where the accumulating FI and their interpenetrating connection form networks [26,37,38]. The growing ICOI over a longer range is likely to establish the backbone (solid-like) structure of an MG. The following shows that this elevates the shear modulus of the glass G as a result. It also shows that the percolation of such networks marks a turning point in the escalating G. This is analogous to the previous observation that the percolation of icosahedra (or quasi-crystal-like) SRO correlates with the plastic localization in a model MG [39,40].

The strong configurational dependence of G in MGs has been discussed before [30–32]. MGs produced with slower cooling rate (termed "older" glasses [31]) exhibit higher G than those obtained with faster cooling rate (termed "younger" glasses [31]). The observation in Fig. 7 confirms this conclusion, showing that G increases markedly with decreasing cooling rate. The three decomposed components of G are also consistent with previous findings: the Born terms (G^{III}) and kinetic contribution (G^{II}) are almost independent of configurations obtained via different quench rates (only slight changes for G^{III} due to the different densities from the Debye–Grüneisen effect of thermal expansion for an isolated configuration state [30,41]). In contrast, the fluctuation term G^{I} is very sensitive to the state of the glass (younger and older) and constitutes almost all the cooling rate dependence of the total G [31,32]. As discussed in the PEL picture in Ref. [31], while the Born term measures the average of the instantaneous curvature of the PEL basin, the majority of the configurational dependence comes from G^{I}, which is the fluctuation of instantaneous slope of the potential energy surface being sampled.

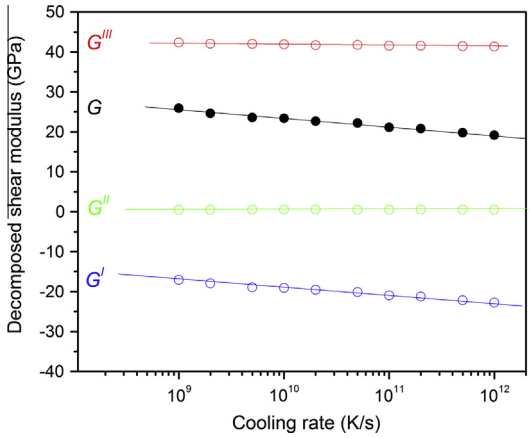

Fig. 7. The shear modulus (G) and the decomposed components (G^{I}, G^{II} and G^{III}), for $Cu_{64}Zr_{36}$ MGs prepared using different cooling rates. (The solid lines serve as guide for the eye.)

Fig. 8 maps the local shear modulus for a typical slice of the $Cu_{64}Zr_{36}$ MG (cooling rate 10^9 K s^{-1}, thickness of average atomic spacing ~2.5 Å). Apparently, the local shear modulus at the coarse-grained scale (see Section 2) is spatially inhomogeneous, and certain regions can be relatively unstable, which is consistent with previous observations [32,33]. The system average is $G = 25.8$ GPa, as indicated by the arrow in the scale bar. Meanwhile, in Fig. 8, the distribution of ICOI networks (only Cu atoms in the center of icosahedra are displayed) is superimposed onto this map. In general, the local G of the cells where ICOI networks reside is well above the bulk average. The ICOI networks can therefore be regarded as an indicator of the most solid-like backbone in the glass structure.

To reveal how ICOI networks develop, Fig. 9 correlates the largest size of the ICOI networks (represented by the

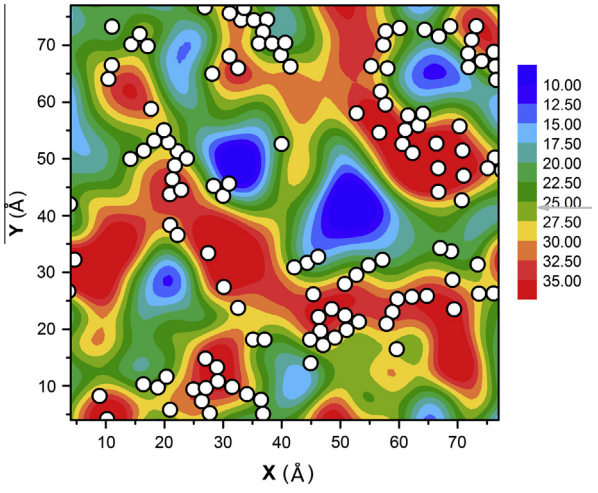

Fig. 8. The distribution of percolated ICOI networks (only the center Cu atoms of full icosahedra are displayed, marked by white open circles) overlapped with a coarse-grained map of local elastic moduli (C_{44}), within a slice (thickness = 2.5 Å) of $Cu_{64}Zr_{36}$ MG cooled to room temperature at 10^9 K s^{-1}. The gray arrow in the scale bar indicates the system-average shear modulus ($G = 25.8$ GPa).

number of the center Cu atoms within the FI in the network), with the fraction of Cu-FI present in the glass. The data points from left to right correspond to samples produced with faster to slower cooling rates: the "younger" glass contains fewer FI and vice versa. The two insets in the figure illustrate the typical ICOI networks in the two corresponding states: the left one shows the four largest ICOI networks (~100–200 FI each); the right one contains a very large ICOI network (~5000 FI). Apparently, there is no percolated FI network within the former configuration, while for the latter sample the largest ICOI network permeates through the whole box. There is a turning point, a threshold of percolation of ICOI networks, P_c which is marked by the yellow region in Fig. 9. P_c for the alloy can be approximated as $P_c \approx 26\% \times 0.64 = 0.166$. Samples on the left only contain separated ICOI networks, and they extend to connect through the whole sample on the right of the percolation.

Next, the CPE dependence of the G is examined for the $Cu_{64}Zr_{36}$ MG. Previous simulation [30] and experiment results [42,43] have reported an almost linear relation between the G and CPE (lower CPE corresponds to higher G). However, in Fig. 10a, two separate regions of the $G \sim$ CPE scaling are observed: the nearly linear relationship holds for both regimes, but with different slopes. Clearly, a turning point exists: the slope is ~ -233 GPa $(\text{eV atom}^{-1})^{-1}$ on the left but almost doubled (~ -450 GPa $(\text{eV atom}^{-1})^{-1}$) on the right. In Fig. 10a, one can observe that this change of slope corresponds to the ICOI network percolation threshold. This can also be viewed from the structural ordering perspective, as there is an almost linear relationship between CPE and fraction of Cu-centered

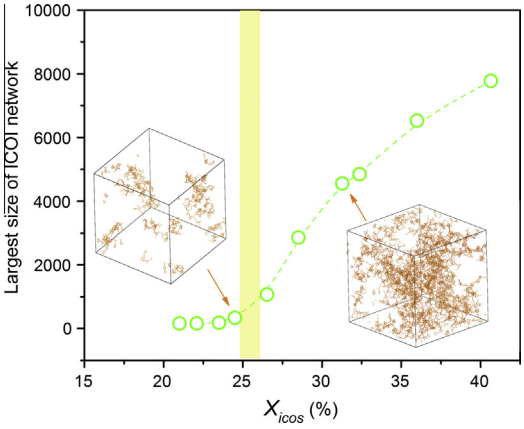

Fig. 9. Relationship between the largest size of ICOI network (the number of center Cu atoms involved in the largest network within the simulation box) and the fraction of Cu-FI in $Cu_{64}Zr_{36}$ MGs. These glassy samples were made from liquids cooled at different quench rates (slower to faster cooling rate: from right to left). The yellow bar marks the percolation of ICOI networks. The left inset exhibits the four largest (but separated) ICOI networks in the system, while the right inset shows only one ICOI network, a large one made up of many (percolated) smaller networks that extends across the periodic boundaries. (For interpretation of the references to color in this figure legend, the reader is referred to the web version of this article.)

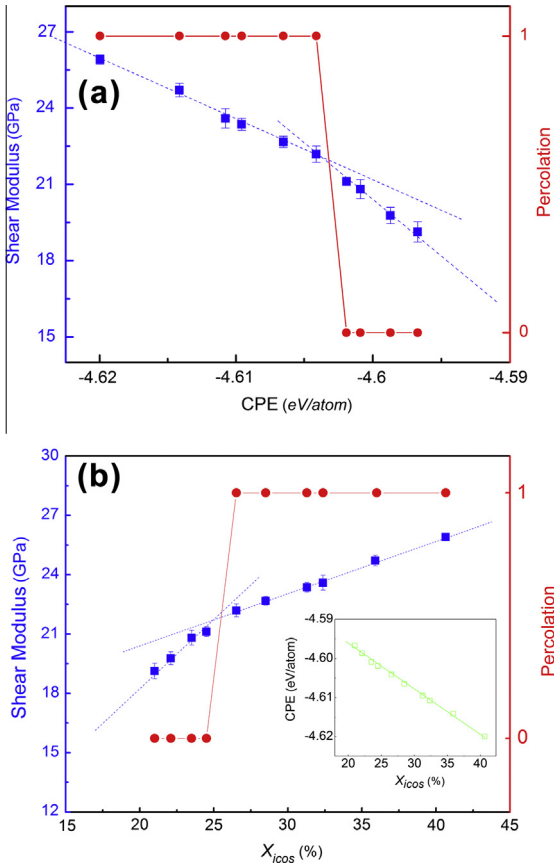

Fig. 10. (a) Correlation between the shear modulus and the CPE of $Cu_{64}Zr_{36}$ MGs. An obvious change in slope is observed around the percolation threshold of the ICOI networks. (b) Correlation between the shear modulus and the fraction of Cu-centered full icosahedra in $Cu_{64}Zr_{36}$ MGs. A change in slope is observed around the percolation threshold of the ICOI networks. Inset shows the correlation between the CPE and X_{icos}.

icosahedra; see the inset in Fig. 10b, which plots the fraction of Cu-centered icosahedra against G. G increases monotonically with increasing FISRO, corresponding to aging the glass to lower CPE (Fig. 10b). As expected, again two regions are observed crossing at the P_c. This observation is similar to the percolation effect of elastic modulus within composite materials [44,45].

This indicates that ICOI is a key structural origin of the increasing system G, and this increase slows down after the ICOI networks percolate. From the PEL perspective, G and the corresponding energy barrier W in Johnson–Samwer's cooperative shear model [43] are sensitively dependent on the configuration. The finding here highlights the role of the icosahedral networks as the backbone structure, and the sensitivity is especially high if the glass structure contains only unlinked ICOI segments.

The observation of this turning point underscores the need to sample the glass configurations over a sufficiently wide range. Specifically, the simulation work by Duan et al. [30] only covered rapid cooling rates above 10^{12} K s^{-1}, and the experimental samples in the laboratory [42,43] only dealt with well-aged glass configurations.

Either one, while each revealing a linear relationship, stays entirely on one side (either left or right) of the P_c in terms of structural development. The point is that G has an explicit FISRO/ICOI dependence, over a wide range of FISRO development, but with different stages before and after ICOI percolation. The backbone role of ICOI networks is thus obvious.

4. Five additional issues regarding FISRO in metallic glasses/liquids

This section discusses five additional (and frequently asked) questions that are directly related to the theme of FISRO. The analysis above allows these issues to be addressed in a coherent fashion.

4.1. FISRO vs. fivefold bonds

As mentioned in Section 1, the literature may have generated the impression that the most general feature in MGs and liquids is ISRO. But the definition of ISRO claimed by different authors is not the same, and this is often where confusion arises. Some authors used the term "icosahedral order" in a more loosely defined way, compared with the FISRO. For example, the preponderance of "fivefold bonds", based on the number of 555 pairs from common neighbor analysis (CNA) or of 1551 pairs (Honeycutt–Andersen index), has been taken as evidence of icosahedral order [46,47]. However, it should be clarified that almost all the preferred clusters in any MGs/liquids would have high fractions of fivefold bonds (and thus high fractions of 555 or 1551 pairs). This can been seen directly from the Voronoi indices of the Frank–Kasper clusters (the Z clusters [8,25]), which are the preferable motifs at different CN in various MGs/liquids. Unlike fcc/hcp, for which the Voronoi index is $\langle 0,12,0,0\rangle$, here, the third number in the Voronoi indices indicating the number of pentagon faces is appreciably larger than the other face types. For example, for $\langle 0,3,6,0\rangle$ for CN = 9, $\langle 0,2,8,0\rangle$ for CN = 10, all the way to $\langle 0,0,12,4\rangle$ for CN = 16, the five-edged faces are always the most populous. The n-edged polygon between the bonding atoms is usually associated with n common neighbors surrounding the pair, and such a configuration would constitute an "n-fold bond" local environment reflected by the CNA index. In other words, fivefold bonds are significant across the board, including for Zr in $Cu_{64}Zr_{36}$ (CN = 16) and for Cu in Zr-rich Cu–Zr MGs (CN = 10), and even in trigonal-prism type metal–metalloid glasses (CN = 9). Obviously, in these amorphous alloys none of the characteristic motifs is actually an icosahedron. Also, in previous reports on dense random packing of hard spheres or monatomic metallic liquids, the fivefold bonds were found populous, and other bond orientational order parameters [48] also suggest high icosahedral order, but the fraction of $\langle 0,0,12,0\rangle$ full icosahedra is not high in those cases, because the majority of the fivefold bonds is in the fragmented icosahedra or icosahedral-like polyhedra. Therefore, on the level of packing motifs in terms of quasi-equivalent $\langle 0,0,12,0\rangle$, the FISRO dominates only in some amorphous alloys at certain compositions (here Cu-rich Cu–Zr). However, the polytetrahedral packing principles, encouraging fivefold bonds and triangulated shell faces, are generally applicable to all MGs and liquids [8]. The polytetrahedral packing includes FISRO (and other types of ISRO people report), but the full icosahedral order per se should not be considered universal.

For $Cu_{64}Zr_{36}$, the preponderance of $\langle 0,0,12,0\rangle$ Cu-FI can also be appreciated from the standpoint of an appropriate effective atomic size ratio [11]. For Cu surrounded by Cu only, the atomic size ratio is 1, and for Cu surrounded by Zr only, the atomic size ratio is ~0.82. In either case, the size ratio is not close to 0.902. In an Cu–Zr alloy, Cu is surrounded by both Cu and Zr, and, at a certain alloy composition, the Cu:Zr ratio is such that the effective size ratio is close to 0.902 for the center atom relative to the average of 12 (Cu + Zr) neighbors. This appears to be the situation near $Cu_{64}Zr_{36}$.

4.2. Can the structure be dissected from a different perspective?

For the MG/liquid alloy, can the structure be analyzed from the perspective of an average atom? First, note that MG-forming liquids and MGs contain as least two constituent elements. In other words, unlike monatomic systems, now one has two intrinsically different local environments that follow the packing principles underlying the structure formation. In $Cu_{64}Zr_{36}$, the average CN around Cu is ~11.8, while that around the larger Zr is ~15.3 (increasing towards 16 on relaxation). The advantage and importance of viewing the structure from the perspective of each species is that Cu- and Zr-centered clusters have very different center-to-shell atomic size ratio, and thus very different CN and local topological order. The information about the respective local environment is contained in the Cu-centered and Zr-centered partial pair-distribution functions (PDF).

If, instead, one elects to view the structure from the standpoint of an average atom (total PDF), the average CN would be ~13. That may result in the misleading conclusion that the local packing is dictated by CN = 13 polyhedra and that icosahedra and Z16 Kasper clusters are not important (or do not even exist).

One can of course take a Zr-centric view; from the minority Zr standpoint, the popular structural motif has been found to be the Z16 cluster, $\langle 0,0,12,4\rangle$, as revealed in the prolonged simulation in Section 3. For Zr, CN is approaching 16 (and 13, for an average atom in the system). The CN is obviously away from the 12 needed for the FI to be the dominant topology. As such, FISRO featuring Cu-FI is prevalent only for Cu-centered local packing, not for Zr surroundings or for the global average. Also note that at Zr-rich Cu–Zr compositions, even for the Cu

local environment FI would not be the most populous polyhedra either, as the average CN around Cu shifts to ~10–11, as elaborated further in Section 4.5. The advantage of singling out Cu-FI is that one can make the point that there is a preferential, and in fact dominant, FISRO scheme around Cu in Cu-rich Cu–Zr alloys, and this particular FISRO is special in that it has consequences for the stability, rigidity, dynamics and rheological properties (see Section 4.3).

4.3. Why do we prefer to characterize the $Cu_{64}Zr_{36}$ structure as FISRO dominated?

This section discusses further the rationales behind choosing Cu-FI as the characteristic SRO. First, Cu is the majority constituent element in the $Cu_{64}Zr_{36}$ alloy. In addition, there is this often-used argument that icosahedra with the fivefold rotational symmetry are incompatible with the long-range translational crystal order. This "dilemma" leads to a barrier for the transition from the icosahedral packing in the amorphous state to the long-range ordered crystals [10,13,47], thus stabilizing the glass against crystallization. The main reason, however, is the mounting evidence contributed by the present authors, which indicates that this particular FISRO based on Cu environments is highly effective in accounting for the properties of the Cu–Zr MGs/liquids [8].

The results presented in Section 3 indicate that Cu-FI help to build the backbone of the $Cu_{64}Zr_{36}$ structure. Cu-FI reach ~40% (compared with 17% for Zr $\langle 0,0,12,4\rangle$ motifs), and all the atoms involved in these FI account for as much as ~90% of the total Cu + Zr atoms. Cu-FI are therefore indeed predominant. It was shown that Cu-FI brings down CPE (see Figs. 1b and 2b), as it involves less free volume and atomic stress [49], and has a uniform CN and fivefold bonds only. Their interconnections evolve with undercooling, in favor of FS, more so than non-icosahedral motifs. The rising shear modulus scales directly with the population of Cu-FI, in particular with ICOI and its spatial distribution, exhibiting a slope change when the ICOI networks percolate.

In addition, previous studies [8] revealed that that Cu prefers more unlike neighbors, owing to the negative heat of mixing, i.e. chemical SRO. In elastic deformation [21], it was shown that Cu-FI offer the highest resistance (lower elastic strain, higher anisotropy index), more than any other type of motifs, including those centered around Zr, and thus representing the regions with higher solidity (lower liquidity) [23]. The correlation with the propensity for non-affine shear transformations is also noteworthy [50,51]: the local regions that exhibits more plastic deformation correlates statistically with those that contain the least Cu-FI. Moreover, atoms associated with Cu-FI show lower mobility in the supercooled liquid [52]. In the liquid, the rise of Cu-FI population coincides with the rising relaxation time, thus controlling the dynamic slowdown with supercooling [20,35,52]. This is supported by the scaling between bond breaking delay time and the Cu-FI fraction (see Fig. 3). Tracking the behavior of Cu thus adequately reflects the response of the system.

4.4. What happens at alloy compositions where Cu-FI is not dominant?

As already emphasized in Section 4.1, although ISRO has been claimed in many of the published papers on MG/liquid structures, and while fivefold bonds are indeed ubiquitous and populous, the FISRO dominates only in a limited number of alloys (at certain MG compositions). Even for other compositions in the Cu–Zr system, such as those on the Zr-rich side, FI are not the most populous motifs [8,52]. Other characteristic local motifs are better suited for describing the amorphous structure, as demonstrated before in many other amorphous alloy systems, including Al-based MGs (solute-centered quasi-equivalent clusters) [53], Mg-based MGs [35] and metal–metalloid MGs [6,20,54], where the preferred characteristic coordination polyhedra are prism-like (such as tri-capped trigonal prism and bi-capped square anti-prism).

As outlined in a recent review [8], at various CN and compositions, there are still featured Kasper polyhedra, which the present authors call Z-clusters. Each type in this variety of polytetrahedral packing schemes still represents a particular preferred motif (although the Kasper cluster type may allow a few quasi-equivalent variations that are slightly distorted and have slightly different make-ups of the shell atoms), for a given atomic size ratio. It is yet to be determined whether any Z-cluster can be as dominant and as energy favorable as Cu-FI in the alloy discussed in this paper. The roles of these Z-clusters in controlling properties also need systematic studies.

4.5. Should one care about the cluster types that are the furthest away from FI?

The answer is yes, even though such unfavorable local structures are of low population in the as-prepared amorphous metals [50]. These are the least ordered local structures and the most "liquid like" [9,23,55], in the spectrum of the inherently inhomogeneous glass structure. There are many occasions when one should pay attention to the "fragmented" and uncomfortable local environments, at the opposite extreme from FI. This is because such local environments can be relevant or even controlling for certain important properties. For example, they are expected to be the most "flexible", i.e., the fertile sites where shear transformations would tend to take place, when the amorphous alloy is imposed to applied stresses [50,51]. Therefore, for improving plastic flow, an adequate fraction of the liquid-like sites [50], rather than focusing on the solid-like backbone, is more desirable. They are obviously of interest, if the objective is to identify the local structures most prone to change, or most likely to respond to external stimuli (such as stress or temperature). However, a detailed

discussion of these high-liquidity [35,55] local regions is beyond the scope of the present paper, and will be the focal point of the next step on fertility index and structure–relaxation relations.

Finally, the present authors point out a misconception that can sometimes be misleading in the community. While in the discussions (and in the literature) the amorphous structure is dissected and described in terms of clusters and motifs, one should not perceive the structure as a composite of "clusters and empty space". Instead, unlike oxide glasses [56] or polymer glasses [57], amorphous metals are atomic glasses. Each atom is the center of its own coordination polyhedron. The non-directional metallic bonding entails space-filling, leading to a continuous spectrum of generally high local packing densities (and usually rather high CN), without bifurcation into connected (or even separated) cluster units (or molecules) plus "holes".

5. Concluding remarks

Although icosahedral order in metallic liquids/glasses has been studied by many researchers since Frank's first proposition in 1952 [12], it is still a topic under ongoing debate. The answers to many important questions are still vague or (seemingly) inconsistent. This is partly due to the intrinsic complexity of the problem (there are many different metallic-glass forming systems involving virtually all common metals in a variety of compositions), and partly due to the lack of consensus on what can be called "icosahedral order" (although the ideal icosahedron is unambiguously defined, the real icosahedra in a liquid/glass are always distorted to some extent, leaving ambiguities in setting the "tolerance" for the distortion before the local environment is designated to be a different polyhedron). This is often the root of the inconsistencies and misconceptions found in recent literature.

The present paper has clarified several issues related to the definition and description of icosahedral order in metallic liquids/glasses, particularly the full icosahedra recently employed to characterize the structure and structure–property relations in certain Cu–Zr amorphous systems. The connections and differences between the ideal icosahedra, full icosahedra, icosahedra-like or significantly distorted icosahedral clusters (asoften used in literature), and the fivefold bonds (as obtained from the CNA or the HA index) generically populous in various types of Z clusters, have been discussed. Further, the icosahedral order is understood in a more general context, which is the polytetrahedral packing featured by the Frank–Kasper polyhedra (Z-clusters): a full icosahedron can be classified as the Z12 cluster (CN = 12) with complete fivefold bonds and no disclination (i.e. highest rotational symmetry), whereas other Z-clusters with larger or smaller CN (corresponding to greater atomic size mismatch) contain the maximum possible number of fivefold bonds and minimum inevitable/intrinsic disclinations for the given CN [8]. In general, the SRO in metallic liquids/glasses is polytetrahedral in nature, and which Z-cluster(s) are favored depends on the relative atomic size of the constituent elements, as well as their chemical SRO. FISRO is dominant only when the appropriate atomic size ratio is reached, such as in $Cu_{64}Zr_{36}$.

Full icosahedra do play an important and distinctive role, at least in Cu-rich Cu–Zr alloys, as recently reported in the literature and further highlighted in the current work. By conducting more systematic simulations, the present authors have revealed additional details regarding the evolution of FISRO with extended relaxation, the conversion of sharing schemes between neighboring icosahedral clusters, the formation of spatial connection and percolation over a longer length scale, and their impact on various properties such as configurational potential energy, specific heat, bond lifetime and local shear modulus. Analysis is also conducted from the Zr-centric view, based on which the present authors rationalize why Cu-centered full icosahedral ordering in this alloy is the telltale indicator that one should focus on. Full icosahedra are important not only because they are dominant in terms of population, but also for how this local order can be directly and effectively connected with some key responses and behaviors of the alloy system. Also of importance is the group of coordination polyhedra that are the least ordered and the most likely to change their configurations; a discussion on that topic will be presented in a separate publication. Such concrete correlations, which the present authors have been actively pursuing over the past several years, will eventually pave the way towards a thorough understanding of structure–property relations for metallic glasses.

Acknowledgements

This work was supported by the Office of Basic Energy Sciences, US Department of Energy (J.D. and E.M. by the Division of Materials Sciences and Engineering, under Contract No. DE-FG02-09ER46056, and Y.Q.C. by the Scientific User Facilities Division).

References

[1] Klement W, Willens RH, Duwez P. Nature 1960;187:4740.
[2] Chaudhari P, Turnbull D. Science 1978;199:4324.
[3] Johnson WL. MRS Bull 1999;24:10.
[4] Greer AL, Ma E. MRS Bull 2007;32:611.
[5] Inoue A. Acta Mater 2000;48:279–306.
[6] Sheng HW, Luo WK, Alamgir FM, Bai JM, Ma E. Nature 2006;439:419.
[7] Miracle DB. Nat Mater 2004;3:697.
[8] Cheng YQ, Ma E. Prog Mater Sci 2011;56:379–473.
[9] Egami T. Prog Mater Sci 2011;56:637–53.
[10] Nelson DR, Spaepen F. Solid State Phys – Adv Res Appl 1989;42:1–90.
[11] Miracle DB. Acta Mater 2006;54:4317–36.
[12] Frank FC. Proc Roy Soc Lond Ser A – Math Phys Sci 1952;215(1120):43–6.
[13] Shen YT, Kim TH, Gangopadhy AK, Kelton KF. Phys Rev Lett 2009;102:057801.

[14] Holland-Moritz D, Herlach DM, Urban K. Phys Rev Lett 1993;71:1196.
[15] Hirata A, Guan PF, Fujita T, Hirotsu Y, Inoue A, Yavari AR, et al. Nat Mater 2011;10:28.
[16] Hirata A, Kang LJ, Fujita T, Klumov B, Matsue K, et al. Science 2013;341:376.
[17] Yang L, Guo GQ, Chen LY, Huang CL, Ge T, et al. Phys Rev Lett 2012;109:105502.
[18] Liu ACY, Neish MJ, Stokol G, Buckley GA, Smillie LA, et al. Phys Rev Lett 2013;110:205505.
[19] Cheng YQ, Ma E, Sheng HW. Phys Rev Lett 2009;102:245501.
[20] Ding J, Cheng YQ, Sheng HW, Ma E. Phys Rev B 2012;85:060201.
[21] Ding J, Cheng YQ, Ma E. Appl Phys Lett 2012;101:121917.
[22] Li MZ, Wang CZ, Hao SG, Kramer MJ, Ho KM. Phys Rev B 2009;80:184201.
[23] Ding J, Cheng YQ, Ma E. Acta Mater 2013;61:4474–80.
[24] Sha ZD, Feng YP, Li Y. Appl Phys Lett 2010;96:061903.
[25] Nelson DR. Phys Rev B 1983;28:5515–35.
[26] Wakeda M, Shibutani Y. Acta Mater 2010;58:3963–9.
[27] Allen MP, Tidesley DJ. Computer simulation of liquids. Oxford: Clarendon Press; 1989.
[28] Mendelev MI, Kramer MJ, Ott RT, Sordelet DJ, Yagodin D, Popel P. Philos Mag 2009;89:967–87.
[29] Voronoi G, Reine J. Angew Math 1908;134:198–287.
[30] Duan G, Lind ML, Demetriou MD, Johnson WL, Goddard III WA, Çain T, et al. Appl Phys Lett 2006;89:151901.
[31] Cheng YQ, Ma E. Phys Rev B 2009;80:064104.
[32] Mayr SG. Phys Rev B 2009;79:060201.
[33] Yoshimoto K, Jain TS, Workum KV, Nealey PF, Pablo J. Phys Rev Lett 2004;93:175501.
[34] Tsamados M, Tanguy A, Goldenberg C, Barrat JL. Phys Rev E 2009;80:026112.
[35] Ding J, Cheng YQ, Ma E. Acta Mater 2013;61:3130–40.
[36] Iwashita T, Nicholson DM, Egami T. Phys Rev Lett 2013;110:205504.
[37] Lee M, Lee CM, Lee KR, Ma E, Lee JC. Acta Mater 2011;59:159–70.
[38] Soklaski R, Nussinov Z, Markow Z, Kelton KF, Yang L. Phys Rev B 2013;87:184203.
[39] Shi YF, Falk ML. Phys Rev Lett 2005;95:095502.
[40] Shi YF, Falk ML. Phys Rev B 2006;73:214201.
[41] Lind ML, Duan G, Johnson WL. Phys Rev Lett 2006;97:015501.
[42] Harmon JS, Demetriou MD, Johnson WL. Appl Phys Lett 2007;90:131912.
[43] Johnson WL, Demetriou MD, Harmon JS, Lind ML, Samwer K. MRS Bull 2007;32:644.
[44] Dufresne A, Cavaillé JY. J Polym Sci: B 1998;36:2211–24.
[45] Favier V, Dendievel R, Canova G, Cavaillé JY, Gilormini P. Acta Mater 1997;45:1557–65.
[46] Clarke AS, Jónsson H. Phys Rev E 1993;47(6):3975–84.
[47] Luo WK, Sheng HW, Alamgir FM, Bai JM, He JH, Ma E. Phys Rev Lett 2004;92:145502.
[48] Steinhardt PJ, Nelson DR, Ronchetti M. Phys Rev B 1983;28:784.
[49] Cheng YQ, Ding J, Ma E. Mater Res Lett 2013;1(1):3–12.
[50] Cheng YQ, Cao AJ, Ma E. Acta Mater 2009;57:3253–67.
[51] Cheng YQ, Cao AJ, Sheng HW, Ma E. Acta Mater 2008;56:5263–75.
[52] Cheng YQ, Sheng HW, Ma E. Phys Rev B 2008;78:014207.
[53] Sheng HW, Cheng YQ, Lee PL, Shastri SD, Ma E. Acta Mater 2008;56:6264–72.
[54] Sheng HW, Ma E, Kramer MJ. JOM 2012;64:856–81.
[55] Dmowski W, Iwashita T, Chuang CP, Almer J, Egami T. Phys Rev Lett 2010;105:205502.
[56] Guthrie M, Tulk CA, Benmore CJ, Xu J, Yarger JL, Klug DD, et al. Phys Rev Lett 2004;93:115502.
[57] Koyama A, Yamamoto T, Fukao K, Miyamoto Y. J Chem Phys 2001;115:560.